Environmental Science Processes & Impacts

PAPER

View Article Online
View Journal | View Issue

Cite this: *Environ. Sci.: Processes Impacts*, 2018, **20**, 1570

Extending surface enhanced Raman spectroscopy (SERS) of atmospheric aerosol particles to the accumulation mode (150–800 nm)†

Peter N. Tirella,[a] Rebecca L. Craig,[a] Darrell B. Tubbs,[a] Nicole E. Olson,[a] Ziying Lei[b] and Andrew P. Ault*[ab]

Due to their small size, measurements of the complex composition of atmospheric aerosol particles and their surfaces are analytically challenging. This is particularly true for microspectroscopic methods, where it can be difficult to optically identify individual particles smaller than the diffraction limit of visible light (~350 nm) and measure their vibrational modes. Recently, surface enhanced Raman spectroscopy (SERS) has been applied to the study of aerosol particles, allowing for detection and characterization of previously undistinguishable vibrational modes. However, atmospheric particles analyzed *via* SERS have primarily been >1 μm to date, much larger than the diameter of the most abundant atmospheric aerosols (~100 nm). To push SERS towards more relevant particle sizes, a simplified approach involving Ag foil substrates was developed. Both ambient particles and several laboratory-generated model aerosol systems (polystyrene latex spheres (PSLs), ammonium sulfate, and sodium nitrate) were investigated to determine SERS enhancements. SERS spectra of monodisperse, model aerosols between 400–800 nm were compared with non-SERS enhanced spectra, yielding average enhancement factors of 10^2 for both inorganic and organic vibrational modes. Additionally, SERS-enabled detection of 150 nm size-selected ambient particles represent the smallest individual aerosol particles analyzed by Raman microspectroscopy to date, and the first time atmospheric particles have been measured at sizes approaching the atmospheric number size distribution mode. SERS-enabled detection and identification of vibrational modes in smaller, more atmospherically-relevant particles has the potential to improve understanding of aerosol composition and surface properties, as well as their impact on heterogeneous and multiphase reactions involving aerosol surfaces.

Received 18th June 2018
Accepted 9th August 2018

DOI: 10.1039/c8em00276b

rsc.li/espi

Environmental significance

Aerosols act as a surface for heterogeneous reactions and multiphase processes in the atmosphere, which impacts their climate-relevant properties (scattering, absorption, and cloud droplet and ice crystal nucleation). Raman microspectroscopy is able to probe organic and inorganic functional groups at ambient temperature and pressure, but is challenging to apply to aerosols critical to climate since the most abundant sizes by number in the atmosphere (~100 nm) are smaller than the diffraction limit of visible light. We show that surface enhanced Raman spectroscopy (SERS) can extend analysis of atmospheric particles down to 150 nm, revealing new chemical detail about accumulation mode particles in the atmosphere and the potential to enable future studies of the complex chemistry occurring at aerosol surfaces.

1 Introduction

Atmospheric aerosol particles impact climate by scattering and absorbing solar radiation and acting as cloud condensation and ice nuclei, which modify cloud properties and precipitation.[1–8] However, these impacts are difficult to quantify due to the complex physicochemical properties of aerosols,[8–10] particularly in terms of chemical composition and mixing state.[9,11–19] This is complicated by the fact that individual particles can contain hundreds to thousands of different chemical species from difference sources and atmospheric aging.[8] An important example of aerosol chemical complexity is secondary organic aerosol (SOA), which forms when low volatility oxidation products of volatile organic compounds (VOCs) condense onto or heterogeneously react with existing aerosol particles containing inorganic salts (*e.g.* ammonium sulfate).[20–22] Though it is known that these particles contain both organic and inorganic components, particle-to-particle variability in chemical

[a]*Department of Chemistry, University of Michigan, Ann Arbor, Michigan, 48109, USA. E-mail: aulta@umich.edu*

[b]*Department of Environmental Health Sciences, University of Michigan, Ann Arbor, Michigan, 48109, USA*

† Electronic supplementary information (ESI) available. See DOI: 10.1039/c8em00276b

composition and mixing state due to different multiphase processes in the atmosphere are not well understood.[20,23,24] In addition, aerosols can have intraparticle chemical variability through processes such as liquid–liquid phase separations.[24–28] More detailed investigations of particle chemical composition and surface properties are needed to improve understanding of multiphase processes,[29,30] such as heterogeneous reactions occurring on surfaces,[31–33] water uptake,[34,35] viscous particles,[36–38] phase transitions,[39,40] and gas-particle partitioning.[41,42]

Over the past decade, Raman microspectroscopy has been increasingly applied as an analytical technique for chemical characterization of aerosol particles.[9,43–46] This technique uses inelastically scattered light to detect vibrational modes present within a sample, which can then be used to identify functional groups and chemical species. Raman microspectroscopy has been applied to characterize many different particle types, such as sea spray and other marine aerosol,[44,47–49] soot and elemental carbon (EC) particles,[50–53] mineral dust,[53–56] and SOA,[46] as well as specific compounds commonly found in aerosols, including biological molecules[57] and various organic compounds like organic nitrates,[58] organosulfates,[59] and glyoxal oligomers.[60] Raman analysis has also been used to study hygroscopic properties,[61–65] phase separations,[66–68] heterogeneous reactions,[49,69,70] ice nucleation,[71] and acidity of aerosols.[72,73] Advantages of this technique include minimal sample preparation and non-destructive analysis under ambient temperature and relative humidity (RH) conditions. However, detection limits in terms of both particle size and analyte concentrations can make Raman microspectroscopic studies of aerosol particles challenging. The majority of aerosol particles, particularly those with long atmospheric lifetimes that react and undergo atmospheric processing, are smaller than 1 μm, but Raman microspectroscopy has been applied mostly to the study of individual particles larger than 1 μm, often 10–30 μm, because it is difficult to optically distinguish smaller particles due to the wavelengths commonly used for Raman analysis (532 or 640 nm) and the diffraction limit of optical microscopy (300–400 nm). Furthermore, even in supermicron atmospheric particles, chemical species are often present in very low concentration, making it difficult to detect Raman signal with enough intensity to determine the identity of vibrational modes and corresponding functional groups. Lastly, important particle properties, such as deliquescence relative humidity can be size-dependent, limiting the ability to translate studies on large particles to atmospherically relevant sizes.[74] If SERS can be used to overcome the detection limit challenges associated with small particle sizes, the potential for Raman microspectroscopic analysis of aerosol particles to improve understanding of chemical composition and mixing state will greatly increase.

Surface enhanced Raman spectroscopy (SERS) has been used to improve the limit of detection of low concentration chemical species,[75] all the way to single molecules.[76] Through SERS, weak Raman signals are enhanced *via* interactions with localized surface plasmon resonances (LSPRs), which are generated by excited electrons in metallic substrates.[75,77–80] The metallic substrates are often silver, gold, or copper and can be in the form of foils, geometric nanoparticles, and colloids.[78,80,81] SERS has applications in many different fields, from biosensing to art preservation, and enhancement factors (EFs) for vibrational intensities of analytes that are reported range from 10^2 to 10^{10}.[75,77–80,82,83] The volumes that experience SERS enhancements are small and typically located less than 5–10 nm from a hotspot, which shows the potential to measure submicron particles that are challenging to identify optically, since a detected SERS-enhanced spectrum originates from a such a small area, it most likely corresponds to an individual particle at low substrate loadings (*e.g.* no particle overlap). In the future, SERS hotspots could be used to probe phenomena localized near aerosol surfaces. With SERS, limitations of optically distinguishing particles for analysis and detection of chemical species present in trace amounts within aerosol particles can be overcome.

Prior to 2015, only a few preliminary, qualitative studies had used SERS for aerosol analysis, with a focus on bioaerosols.[84–86] Since 2015, SERS has been applied to the study of aerosol particles more broadly and in a more quantitative manner. In 2015, Craig *et al.* used silver nanoparticle coated quartz substrates to investigate both ammonium sulfate and sodium nitrate aerosol particle standards, as well as ambient aerosol.[87] In 2016, Fu *et al.* used Klarite, a commercially available substrate of structured gold inverted pyramids, to study mixed ammonium sulfate and naphthalene particles.[88] A few variations of SERS, such as tip-enhanced Raman spectroscopy (TERS),[89] electrospray SERS (ES-SERS),[90] and surface-enhanced resonance Raman spectroscopy (SERRS) of trapped and suspended particles,[91] have also been applied to study aerosol particles. Reported EFs ranged from 2.0–70 for $\nu_s(SO_4^{2-})$, $\nu_s(NO_3^-)$, ν(C–H), ν(O–H), and δ(C–C) vibrational modes[87,88,90] and 10^5 for vibrational modes of rhodamine 590 chloride (R6G), a dye with a large scattering cross-section commonly used for SERS studies.[91] However, most particles probed in these studies were supermicron, not in the submicron size range most abundant for ambient aerosol, and further work is needed to increase EFs for vibrational modes corresponding to more atmospherically-relevant chemical compounds.

In this study, silver SERS substrates, including Ag nanoparticles and commercial Ag foil, were tested with both organic and inorganic species commonly observed in aerosols. Additionally, laboratory-generated and ambient aerosol particles <1 μm were analyzed to explore the lower limit in terms of particle size for SERS using these simple methods. The results of this study highlight the potential for SERS analysis of aerosol particles with atmospherically-relevant sizes (down to 150 nm) to improve understanding of chemical composition, mixing state, and reactions occurring on aerosol surfaces that impact aerosol climate effects.

2 Experimental

2.1 Materials and reagents

Quartz slides (Ted Pella, Inc.) and silver foil (ESPI Metals) were purchased and used as substrates. Silver nitrate ($Ag(NO_3)_2$) (Sigma-Aldrich), hydroxylamine hydrochloride (Sigma-Aldrich), and sodium hydroxide (Fischer) were used for silver

nanoparticle (AgNP) synthesis (described below). Polystyrene latex sphere (PSL) standards (Polysciences, Inc.), ammonium sulfate ($(NH_4)_2SO_4$) (Alfa Aesar), and sodium nitrate (Sigma Aldrich) were used as model aerosol systems. All chemicals were >98% purity and used without further purification.

2.2 Substrate preparation

Quartz coverslips were cut and cleaned prior to use either directly as substrates or as a base for a silver nanoparticle (AgNP) SERS substrates. AgNPs were synthesized by reducing silver nitrate with hydroxylamine hydrochloride, according to the method by Leopold and Lendl.[92] The resulting colloidal solution of AgNPs was drop-coated onto clean quartz slides and dried in a desiccator to create SERS substrates in the same manner as Craig *et al.*[87] Size distribution data collected *via* Nanoparticle Tracking Analysis (NTA)[93–95] for the AgNPs prior to dropcoating is included in the ESI.† Silver foil (0.002″ (0.05 mm) thick, ESPI Metals) was cut for use as SERS substrates. Microscopy characterization of the Ag foil is included in the ESI.†

2.3 Laboratory-generated aerosol particle samples

Organic particle standards were generated by aerosolizing colloidal solutions of PSLs of varying size (400 nm, 600 nm, and 800 nm). Prior studies have analyzed PSLs with SERS going back to the 1990's,[96] providing useful reference points for Raman studies focused on aerosol particles. Inorganic aerosol particle standards were generated by aerosolizing solutions of 30 mM $(NH_4)_2SO_4$ or 30 mM $NaNO_3$. All solutions were made with 18.3 MΩ Milli-Q water. Aerosolization was conducted with a Collison nebulizer operated with HEPA-filtered air and the generated aerosol was passed through two diffusion dryers to remove excess water before being impacted onto substrates with a microanalysis particle sampler (MPS-3, California Instruments, Inc.). Prior to impaction, the inorganic standard particles were size-selected at 400 nm, 600 nm, or 800 nm (electrical mobility diameter) with an electrostatic classifier (Model 3080, TSI Corporation) equipped with a long differential mobility analyzer (Model 3081, TSI Corporation) at sample to sheath flow ratio of 1 : 8.3 (0.3 to 2.5 lpm).

2.4 Ambient aerosol particle samples

Ambient samples were collected from outside the University of Michigan Chemistry Building (42.2783° N, 83.7372° W). Samples were size selected at 150 nm (electrical mobility diameter) with a differential mobility analyzer (Model 3081, TSI Corporation) and then collected on Ag foil *via* impaction with the MPS-3. Each sample was collected for ~1 hour.

2.5 Raman microspectroscopy

Raman analysis was performed with a Horiba Labram HR Evolution Raman spectrometer (Horiba Scientific) coupled to a confocal optical microscope (100× Olympus objective, 0.9 N.A.). The spectrometer was equipped with a Nd:YAG laser source (50 mW, 532 nm) and a CCD detector. A 600 groove per mm diffraction grating yielded spectral resolution of 1.8 cm^{-1}. Calibration was carried out daily against the Stokes Raman signal of a pure silicon standard at 520 cm^{-1}. Laser power was attenuated with neutral density (ND) filters ranging from 1 to 100 to prevent sample damage. Spectra were collected for the range of 500 to 4000 cm^{-1} for 3 accumulations with 15 s acquisition time. 8–15 particles were analyzed for each sample. Raman maps were collected with computer-controlled XY Raman mapping, with spectra recorded using a point-by-point scanning mode with a 0.25 μm step size. Map spectra were also collected from 500 to 4000 cm^{-1} for 3 accumulations with 15 s acquisition time. Each spectrum collected during a map acquisition was matched to its corresponding location in an optical image to determine if it represented an aerosol particle. Samples were exposed to ambient relative humidity and temperature conditions during Raman analysis (~23 °C and 40–60% RH).

SERS EFs were calculated for vibrational modes of interest according to eqn (1). I_{SERS} and I_{RS} are the Raman signal under SERS and non-SERS conditions, respectively, and c_{SERS} and c_{RS} are the analyte concentration under SERS and non-SERS conditions, respectively.[97]

$$EF = \frac{I_{SERS}/c_{SERS}}{I_{RS}/c_{RS}} = \frac{I_{SERS}}{I_{RC}} \quad (1)$$

Since sample preparation for SERS and non-SERS conditions was identical, the concentration c_{SERS} can be assumed to be equal to c_{RS} and the equation to calculate EFs can be simplified to a comparison of I_{SERS} and I_{RC}. I_{SERS} and I_{RC} are represented by the integrated peak area for the respective vibrational modes. Integrated peak areas were determined along the natural baseline of the spectra using a multipeak fitting software package (Igor Pro, WaveMetrics). The average integrated peak area for Raman spectra collected under non-SERS conditions was used for I_{RC}.

3 Results and discussion

Laboratory-generated aerosol particle standards were used to investigate enhancement from various Ag SERS substrates, including AgNP coated quartz and Ag foil, and their application to aerosol particle studies, specifically particles <1 μm. Raman spectra of standard PSL particles sized 400 nm, 600 nm, and 800 nm collected from each substrate showed that, while both Ag SERS substrates enhanced the Raman signal across all vibrational modes, Ag foil yielded significantly higher EFs (Fig. 1). Raman spectra were successfully collected for PSL particles of all sizes on the Ag foil and quartz substrates, but due to low intensity and the resulting small enhancement, only the 800 nm PSLs were tested with the AgNP substrate. Even though Raman signal was detected for PSL particles on plain quartz substrate, intensity was very low and vibrational modes were difficult to distinguish from background noise, particularly for the 400 nm sized particles. For the 800 nm PSL particles, EFs for the symmetric ring stretching modes, ν_s(C–C)[98–100] at 1000 cm^{-1} and ν_s(C=C)[98–100] at 1602 cm^{-1}, ranged for 7 to 32 and 11 to 33, respectively, for the Ag foil and 1 to 4 and 2 to 9 for the AgNP

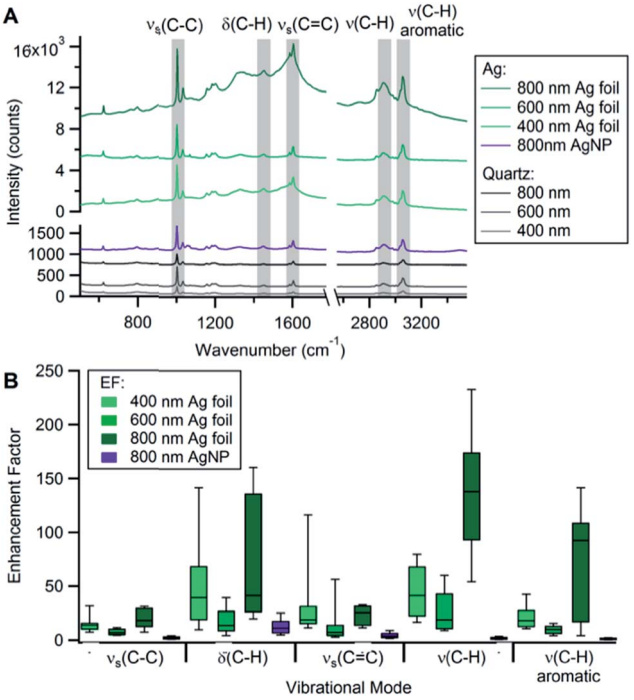

Fig. 1 (A) Average Raman spectra for 400 nm, 600 nm, and 800 nm PSL particles on quartz, Ag foil, and AgNP substrates. (B) Box and whisker plot of calculated EFs for vibrational modes of interest for all particle sizes. The center line represents the median, the box outlines the inner quartiles, and the whiskers represent the 10th and 90th percentile.

substrate, respectively. In comparison to the ring stretching modes, C–H bending and stretching modes showed greater enhancement in response to the SERS effect. EFs for the C–H bending mode (δ(C–H), 1452 cm^{-1}),[98,99] C–H stretching mode (ν(C–H), 2908 cm^{-1}),[98,99] and aromatic C–H stretching mode (ν(C–H) aromatic, 3054 cm^{-1})[98,99] ranged from 20 to 161, 54 to 233, and 4 to 142, respectively, for the Ag foil and 5 to 26, 1 to 4, and 1 to 3, respectively, for the AgNP substrate. The EF values for the AgNP substrate samples are consistent with previously reported EF values for $(NH_4)_2SO_4$ and $NaNO_3$ standard particles analyzed with SERS using similar substrates.[87] SERS enhancement was observed for the 400 and 600 nm sized particles on Ag foil and EFs for the five PSL vibrational modes ranged from 4 to 151, with the δ(C–H) and ν(C–H) modes again exhibiting the largest enhancements. All Raman spectra, for PSL particles on both quartz and Ag foil, are provided in the ESI.† It should be noted that both the 400 nm and 600 nm particles are smaller than the 721 nm diameter of the laser spot (for a 532 nm laser with 0.9 N.A. objective).

The large variability in EFs, particularly evident for the Ag foil samples, could be attributed to varying degrees of coupling between LSPRs with analytes depending on location of the particle with respect to the SERS-enhanced volume on the rough surface of the Ag foil or inconsistent distribution of AgNPs. Preliminary work testing several other Ag SERS substrates is included in the ESI† and results were, at best, comparable to the AgNP enhancement shown here. Despite the variability in enhancement, the Ag foil substrate yielded the highest EFs and thus, was used as the SERS substrate for all subsequent experiments in this work.

Across all vibrational modes, there was no clear relationship between particle size and enhancement. Enhancement was expected to increase with increasing particle size, as the higher number of analyte molecules present in the larger particles could enable more opportunities for coupling to LSPRs and lead to greater enhancement of the Raman signal. This was observed somewhat for the largest and smallest sized PSL particles analyzed, as the 800 nm particles were consistently more enhanced than the 400 nm particles, but the 600 nm particles exhibited the lowest levels of enhancement. The cause for the low enhancement observed for the 600 nm PSL particles is unclear at this time, but could possibly be due to PSL quality, crowding effects, or the arrangement of PSL molecules hindering coupling between LSPRs and analyte molecules. The inorganic particles investigated as part of this study (discussed below) were more consistent with the 400 nm and 800 nm PSL particles, with larger sized particles yielding more enhanced spectra.

In addition to PSL particles, which are primarily organic, $(NH_4)_2SO_4$ and $NaNO_3$ particles were also tested since atmospheric aerosol particles often contain these inorganic components.[101] $(NH_4)_2SO_4$ and $NaNO_3$ particles were generated from solution and size-selected at 400 nm, 600 nm, and 800 nm for SERS analysis. For $(NH_4)_2SO_4$, the $\nu(SO_4^{2-})$ and the ν(N–H) stretching mode of NH_4^+ were studied (Fig. 2). The $\nu_1(SO_4^{2-})$[44,46,47,102,103] mode at 963 cm^{-1} had EFs ranging from 30 to 841, which is up to ~420 times greater than the average EFs reported by Craig *et al.* using AgNP SERS substrates.[87] There was a red shift in peak location for the SERS enhanced $\nu_1(SO_4^{2-})$ mode, shifting from 975 cm^{-1} to 963 cm^{-1}, along with an increase in peak broadness. This shift is possibly attributed to charge-transfer interactions between Ag and the $(NH_4)_2SO_4$ molecules and is consistent with earlier work studying SERS enhancement of $(NH_4)_2SO_4$/sucrose particles.[90] The ν(N–H)[102,103] mode centered at 3130 cm^{-1} had EFs ranging from 33 to 730. It should be noted that ν(N–H) is broader due to hydrogen bonding and can be difficult to quantify in low-intensity spectra. For $NaNO_3$, three stretches corresponding to NO_3^- were studied (Fig. 3). $\nu_1(NO_3^-)$[47,103,104] at 1067 cm^{-1} had EFs ranging from 8 to 48, which is up to ~16 times greater than the average EFs reported by Craig *et al.* using AgNP SERS substrates.[87] There was a slight blue shift in peak location for the SERS enhanced $\nu_1(NO_3^-)$ mode, shifting from 1056 cm^{-1} to 1067 cm^{-1}, along with an increase in peak sharpness. The 1054 cm^{-1} mode corresponds to aqueous, free NO_3^-, while the 1067 cm^{-1} mode corresponds to Na^+-bound NO_3^-.[69,103] Interestingly, this result is inconsistent with previous work that observed a red shift from 1067 cm^{-1} to 1054 cm^{-1} for $\nu_1(NO_3^-)$.[87,105] Previous work proposed that $NaNO_3$ cannot couple as effectively as NO_3^- with the Ag substrate due to interaction with sodium or incorporation into a $NaNO_3$ amorphous solid or crystal, leading to a red shift occurring with increased enhancement.[87] Experimental conditions, such as RH impacts on particle phase, could play a role, but further work is needed to characterize this

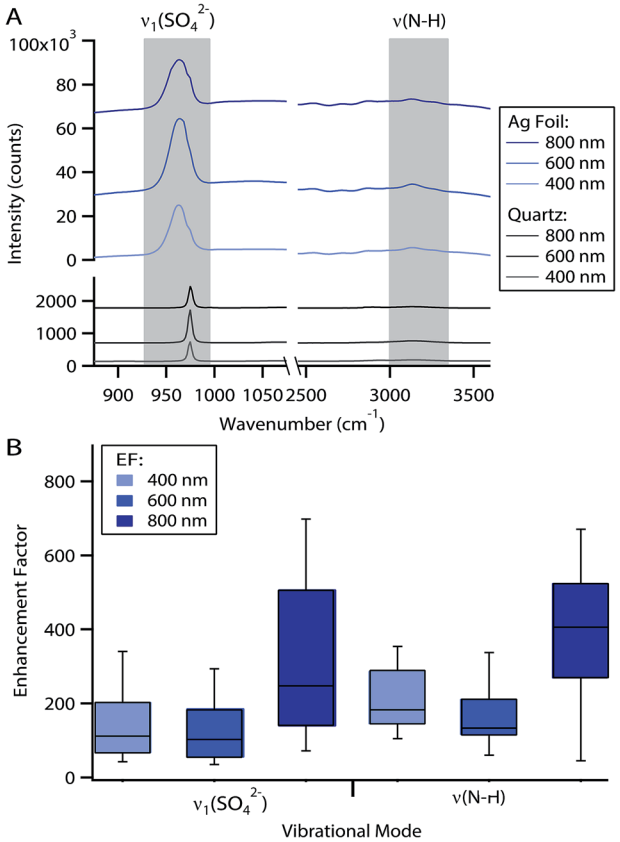

Fig. 2 (A) Average Raman spectra for 400 nm, 600 nm, and 800 nm $(NH_4)_2SO_4$ particles on quartz and Ag foil substrates. (B) Box and whisker plot of calculated EFs for vibrational modes of interest for all particle sizes. The center line represents the median, the box outlines the inner quartiles, and the whiskers represent the 10th and 90th percentile.

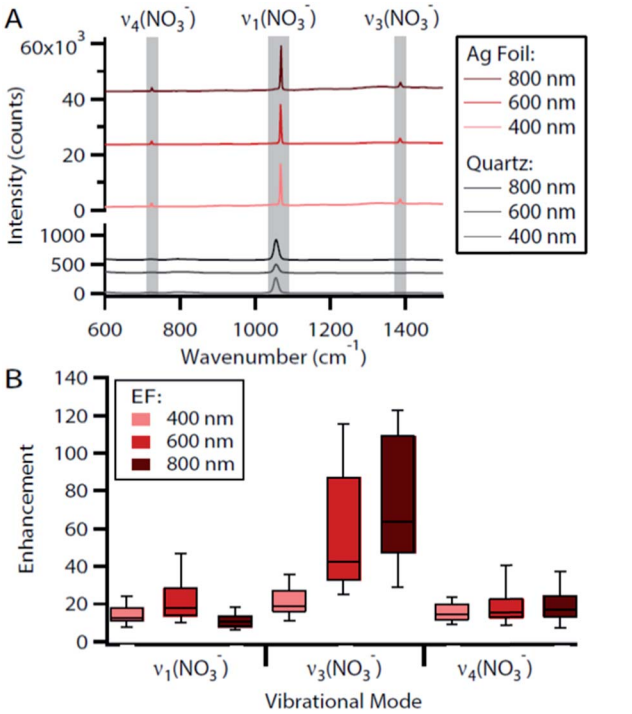

Fig. 3 (A) Average Raman spectra for 400 nm, 600 nm, and 800 nm $NaNO_3$ particles on quartz and Ag foil substrates. (B) Box and whisker plot of calculated EFs for vibrational modes of interest for all particle sizes. The center line represents the median, the box outlines the inner quartiles, and the whiskers represent the 10th and 90th percentile.

phenomenon and reconcile the discrepancy in observed peak shifting. Other modes, $\nu_3(NO_3^-)$[103,104] at 1386 cm^{-1} and $\nu_4(NO_3^-)$[103,104] at 725 cm^{-1}, had larger EFs, ranging from 5 to 116, and no observable peak shifts. All Raman spectra, for $(NH_4)_2SO_4$ and $NaNO_3$ particles on both quartz and Ag foil, are provided in the ESI.†

Qualitative observation shows that EFs increased with increasing particle size for the vibrational modes studied for the 400 nm and 800 nm $(NH_4)_2SO_4$ particles. As discussed previously, this could be attributed to the higher number of analyte molecules present in the larger particles and the greater probability that a portion of the particle would be within the enhanced region of a LSPR after impaction leading to greater observed enhancement. An alternate explanation for increased enhancement is the accumulation of crystals or ions at the foil interface as the aqueous particles spread upon impaction. This effect applies only to the $(NH_4)_2SO_4$ and $NaNO_3$ particles, as the PSL particles are solid. Similar to the PSL particles, the 600 nm $(NH_4)_2SO_4$ particles exhibited the lowest enhancement. There is no apparent trend for the EFs for the vibrational modes studied for all sized $NaNO_3$ particles. Also, as with the PSL particles, there was a high level of variability in enhancement for all of the $(NH_4)_2SO_4$ and $NaNO_3$ vibrational modes. Further testing with more samples, both in terms of particle sizes studied and number of particles analyzed, is necessary to resolve any trends or relationships between particle size and enhancement.

Thus far in this study, through SERS, the smallest particle size shown has been 400 nm, which is about 2–3 times smaller than the size of aerosol particles typically characterized through Raman analysis. However, SERS is capable of single molecule detection and so, should allow for Raman analysis of aerosol particles <400 nm. To test this limit, 150 nm PSL particles were collected on Ag foil. It should be noted that a 150 nm sized particle is well below the diffraction limit of visible light for typical Raman systems, as well as the Raman spectrometer used in this study (300–400 nm and 361 nm, respectively), making individual particle identification challenging. Automated point-by-point mapping with a step size of 0.25 μm was used over a larger region of the substrate, enabling spectra to be collected for the 150 nm particles that were difficult to distinguish optically due to spatial resolution limitations. A representative spectrum for a 150 nm PSL particle and its corresponding location are shown in Fig. 4. The five vibrational modes focused on in the earlier analysis are indicated, though other vibrational modes were also enhanced and present. In the optical image, the yellow box highlights the mapped region, while the red circle indicates the point corresponding to the SERS PSL spectrum. The small, dark spots are individual 150 nm PSL particles, while the larger spots are most likely agglomerates and were

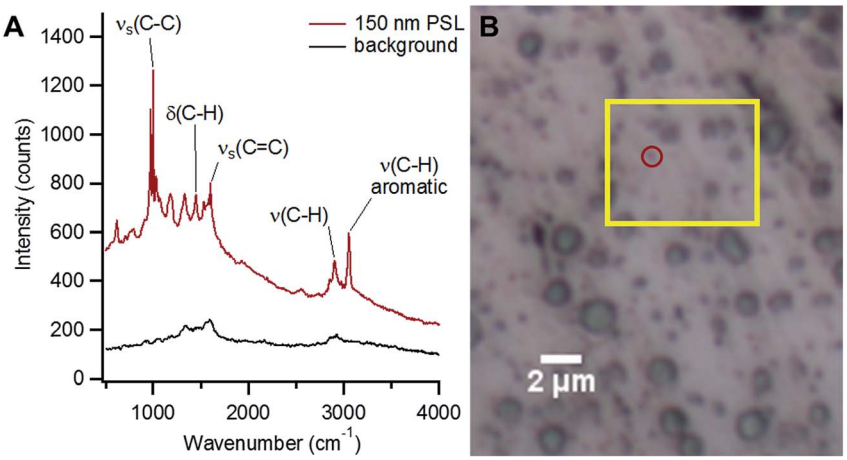

Fig. 4 (A) SERS spectrum collected *via* automated point-by-point mapping of a 150 nm PSL particle on Ag foil substrate. (B) Optical image of 150 nm PSL sample on Ag foil, with the yellow box highlighting the mapped area and the red circle indicating the location of the Raman spectrum shown in (A).

avoided for this analysis. It should also be noted that marks and scratches to the Ag foil can lead to intensity in the Raman spectra that make it difficult to identify vibrational modes corresponding to the particles. To reduce substrate interference, smooth regions of the Ag foil were selected for mapping analysis.

In addition to testing SERS with laboratory-generated aerosol standards below the diffraction limit, ambient aerosol particles were also sampled, size-selected at 150 nm, and impacted in a same manner (Fig. 5). Based on the sampling time and aerosol concentrations, the substrate has primarily individual particles with minimal overlap. While it is difficult to definitively identify vibrational modes in ambient aerosol due to their complex chemical composition and overlapping regions where modes can be present, tentative assignments are proposed. Peaks in the 500–900 cm^{-1} region could correspond to ν(Si–O–Si), δ(Si–O–Al), and other lattice vibrations of fly ash or silicon and aluminosilicate minerals,[54,98,106–108] δ(C–O) of carbonates and carboxylic acids,[54,87,98] or "breathing" modes of aromatic rings.[57] The peaks at 963–988 cm^{-1} most likely correspond to $\nu_1(SO_4^{2-})$,[44,46,47,102,103] and are exhibiting the same red shift observed for the $(NH_4)_2SO_4$ standard particles discussed earlier.[90] Peaks in the 1000–1700 cm^{-1} region could correspond to a range of vibrational modes of organic functional groups, including stretching modes, such as ν(C–O), ν(C–C), ν(C=C), ν(COO$^-$), and ν(C–OH), and bending and twisting modes, such as $\delta(CH_2)$, $\delta(CH_3)$, δ(C–C), δ(O–C–O), and δ(O–H).[44,47,54,57–60,67,98,109,110] Peaks in the higher energy 2700–3000 cm^{-1} region correspond to symmetric and asymmetric $\nu(CH_2)$ and $\nu(CH_3)$ modes.[44,47,54,57,59,98] Specific compounds present in the ambient aerosol particles related to these functional groups could include long chain aliphatics, glyoxal oligomers, peroxides, organic sulfates, and minerals associated with dust.[47,54,59,60,70] To our knowledge, this is the first SERS-enhanced spectroscopic analysis of aerosol particles that have a smaller diameter than the visible light diffraction limit, an important step towards measurements of aerosol particles in a key size range for atmospheric surface chemistry. Additionally, for these ambient spectra, vibrational modes attributed to organic species exhibited greater enhancement in the lower frequency region (1000–1800 cm^{-1}) than the higher frequency region (2700–3000 cm^{-1}), which is consistent with previous work with SERS of ambient particles.[87] This demonstrates the potential for SERS to enable the study of vibrational modes that are not as well characterized in the literature due to the difficulties associated with detecting them in aerosol particles *via* traditional microspectroscopic methods.

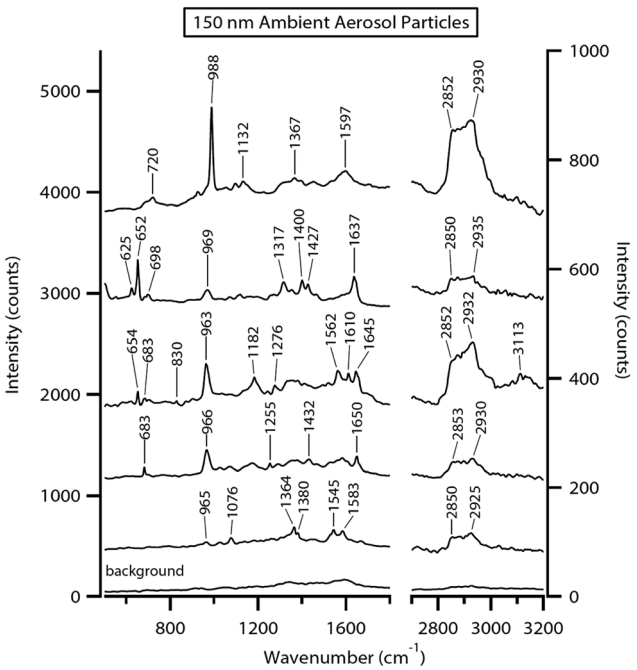

Fig. 5 SERS-enhanced spectra obtained from Raman mapping of 150 nm size-selected ambient aerosol particles.

4 Conclusions

SERS was applied to the study of atmospheric aerosol particles to improve the limit of detection in terms of particles size. 400 nm, 600 nm, and 800 nm size-selected laboratory-generated aerosol particle standards of PSLs, ammonium sulfate, and sodium nitrate were collected on Ag foil SERS substrates and analyzed. Average enhancement factors for a range of inorganic and organic vibrational modes were calculated to be on the order of 10^2 and as large as 530. SERS enhancements may increase with increasing particle size, as observed with the 400 nm and 800 nm PSL and $(NH_4)_2SO_4$ standards, but the 600 nm PSL and $(NH_4)_2SO_4$ particles had the lowest EF values and there was no observed consistent trend between SERS enhancement and particle size for the $NaNO_3$ standard. These results are likely due to variability in LSPRs on the foil surface and subsequent coupling with analyte molecules. Further testing with more particle sizes and increased number of particles analyzed is necessary to resolve a definitive relationship between particle size and enhancement. Ag foil substrates were also used for SERS analysis of 150 nm PSL and ambient aerosol particles *via* automated Raman mapping. All five PSL vibrational modes characterized with the larger sized particles were identified in the SERS enhanced spectra of the 150 nm particles. For the ambient aerosol, a range of inorganic and organic vibrational modes were detected, and corresponding functional groups were proposed. To our knowledge, this is the first vibrational spectroscopic analysis of aerosol particles approaching the mode of the atmospheric number size distribution (~100 nm). These results show the potential for SERS to enable improved analysis of aerosol particle chemical composition and mixing state for the most atmospherically abundant particle sizes. The ability to detect chemical species in these small volume particles also shows the potential for future SERS work to probe differences in composition at aerosol surfaces due to phase separation, the presence of surfactants, or surface-level reactions. Overall, future SERS studies of atmospheric aerosol composition could lead to improved understanding of multiphase atmospheric processing and aerosol impacts on climate and human health.

Conflicts of interest

There are no conflicts to declare.

Acknowledgements

This work was supported by a National Science Foundation CAREER Grant to APA (CHE-1654149) and startup funds from the University of Michigan. RLC was partially supported by the Susan Lipschutz Fellowship Award from the University of Michigan Rackham Graduate School. DBT was partially supported by the Detroit Research Internship Summer Experience (D-RISE) program, funded by the NSF (CHE-1305777) to Dr Nicolai Lehnert at UM, the UM College of Literature, Science and the Arts, the UM Office of the Provost, and Cass Technical High School in Detroit, MI. The Pratt Lab at the University of Michigan is acknowledged for assistance with ambient aerosol sampling.

References

1 L. Di Girolamo, T. C. Bond, D. Bramer, D. J. Diner, F. Fettinger, R. A. Kahn, J. V Martonchik, M. V Ramana, V. Ramanathan and P. J. Rasch, Analysis of Multi-angle Imaging Spectro Radiometer (MISR) aerosol optical depths over greater India during winter 2001-2004, *Geophys. Res. Lett.*, 2004, **31**, L23115, DOI: 10.1029/2004GL021273.

2 U. Pöschl, Atmospheric aerosols: composition, transformation, climate and health effects, *Angew. Chem., Int. Ed.*, 2005, **44**, 7520–7540.

3 M. O. Andreae and D. Rosenfeld, Aerosol-cloud-precipitation interactions. Part 1. The nature and sources of cloud-active aerosols, *Earth-Sci. Rev.*, 2008, **89**, 13–41.

4 P. J. DeMott, T. C. J. Hill, C. S. McCluskey, K. A. Prather, D. B. Collins, R. C. Sullivan, M. J. Ruppel, R. H. Mason, V. E. Irish, T. Lee, C. Y. Hwang, T. S. Rhee, J. R. Snider, G. R. McMeeking, S. Dhaniyala, E. R. Lewis, J. J. B. Wentzell, J. Abbatt, C. Lee, C. M. Sultana, A. P. Ault, J. L. Axson, M. Diaz Martinez, I. Venero, G. Santos-Figueroa, M. D. Stokes, G. B. Deane, O. L. Mayol-Bracero, V. H. Grassian, T. H. Bertram, A. K. Bertram, B. F. Moffett and G. D. Franc, Sea spray aerosol as a unique source of ice nucleating particles, *Proc. Natl. Acad. Sci.*, 2016, **113**, 5797–5803.

5 A. P. Ault, C. R. Williams, A. B. White, P. J. Neiman, J. M. Creamean, C. J. Gaston, F. M. Ralph and K. A. Prather, Detection of Asian dust in California orographic precipitation, *J. Geophys. Res.*, 2011, **116**, D16205.

6 J. M. Creamean, K. J. Suski, D. Rosenfeld, A. Cazorla, P. J. DeMott, R. C. Sullivan, A. B. White, F. M. Ralph, P. Minnis, J. M. Comstock, J. M. Tomlinson and K. A. Prather, Dust and biological aerosols from the Sahara and Asia influence precipitation in the western U.S., *Science*, 2013, **339**, 1572–1578.

7 J. M. Creamean, A. P. Ault, A. B. White, P. J. Neiman, F. M. Ralph, P. Minnis and K. A. Prather, Impact of interannual variations in sources of insoluble aerosol species on orographic precipitation over California's central Sierra Nevada, *Atmos. Chem. Phys.*, 2015, **15**, 6535–6548.

8 K. A. Prather, C. D. Hatch and V. H. Grassian, Analysis of Atmospheric Aerosols, *Annu. Rev. Anal. Chem.*, 2008, **1**, 485–514.

9 A. P. Ault and J. L. Axson, Atmospheric Aerosol Chemistry: spectroscopic and Microscopic Advances, *Anal. Chem.*, 2017, **89**, 430–452.

10 K. A. Prather, T. H. Bertram, V. H. Grassian, G. B. Deane, M. D. Stokes, P. J. DeMott, L. I. Aluwihare, B. P. Palenik, F. Azam, J. H. Seinfeld, R. C. Moffet, M. J. Molina, C. D. Cappa, F. M. Geiger, G. C. Roberts, L. M. Russell, A. P. Ault, J. Baltrusaitis, D. B. Collins, C. E. Corrigan,

L. A. Cuadra-Rodriguez, C. J. Ebben, S. D. Forestieri, T. L. Guasco, S. P. Hersey, M. J. Kim, W. F. Lambert, R. L. Modini, W. Mui, B. E. Pedler, M. J. Ruppel, O. S. Ryder, N. G. Schoepp, R. C. Sullivan and D. Zhao, Bringing the ocean into the laboratory to probe the chemical complexity of sea spray aerosol, *Proc. Natl. Acad. Sci.*, 2013, **110**, 7550–7555.

11 N. Riemer and M. West, Quantifying aerosol mixing state with entropy and diversity measures, *Atmos. Chem. Phys.*, 2013, **13**, 11423–11439.

12 O. S. Ryder, A. P. Ault, J. F. Cahill, T. L. Guasco, T. P. Riedel, L. A. Cuadra-Rodriguez, C. J. Gaston, E. Fitzgerald, C. Lee, K. A. Prather and T. H. Bertram, On the Role of Particle Inorganic Mixing State in the Reactive Uptake of N_2O_5 to Ambient Aerosol Particles, *Environ. Sci. Technol.*, 2014, **48**, 1618–1627.

13 E. Fitzgerald, A. P. Ault, M. D. Zauscher, O. L. Mayol-Bracero and K. A. Prather, Comparison of the mixing state of long-range transported Asian and African mineral dust, *Atmos. Environ.*, 2015, **115**, 19–25.

14 A. P. Ault, C. J. Gaston, Y. Wang, G. Dominguez, M. H. Thiemens and K. A. Prather, Characterization of the Single Particle Mixing State of Individual Ship Plume Events Measured at the Port of Los Angeles, *Environ. Sci. Technol.*, 2010, **44**, 1954–1961.

15 R. M. Healy, N. Riemer, J. C. Wenger, M. Murphy, M. West, L. Poulain, A. Wiedensohler, I. P. O'Connor, E. McGillicuddy, J. R. Sodeau and G. J. Evans, Single particle diversity and mixing state measurements, *Atmos. Chem. Phys.*, 2014, **14**, 6289–6299.

16 R. E. O'Brien, B. B. Wang, A. Laskin, N. Riemer, M. West, Q. Zhang, Y. L. Sun, X. Y. Yu, P. Alpert, D. A. Knopf, M. K. Gilles and R. C. Moffet, Chemical imaging of ambient aerosol particles: Observational constraints on mixing state parameterization, *J. Geophys. Res.*, 2015, **120**, 9591–9605.

17 L. Fierce, T. C. Bond, S. E. Bauer, F. Mena and N. Riemer, Black carbon absorption at the global scale is affected by particle-scale diversity in composition, *Nat. Commun.*, 2016, **7**, 12361.

18 D. B. Collins, A. P. Ault, R. C. Moffet, M. J. Ruppel, L. A. Cuadra-Rodriguez, T. L. Guasco, C. E. Corrigan, B. E. Pedler, F. Azam, L. I. Aluwihare, T. H. Bertram, G. C. Roberts, V. H. Grassian and K. A. Prather, Impact of marine biogeochemistry on the chemical mixing state and cloud forming ability of nascent sea spray aerosol, *J. Geophys. Res.*, 2013, **118**, 8553–8565.

19 A. P. Ault, R. C. Moffet, J. Baltrusaitis, D. B. Collins, M. J. Ruppel, L. A. Cuadra-Rodriguez, D. Zhao, T. L. Guasco, C. J. Ebben, F. M. Geiger, T. H. Bertram, K. A. Prather and V. H. Grassian, Size-dependent changes in sea spray aerosol composition and properties with different seawater conditions, *Environ. Sci. Technol.*, 2013, **47**, 5603–5612.

20 M. Hallquist, J. C. Wenger, U. Baltensperger, Y. Rudich, D. Simpson, M. Claeys, J. Dommen, N. M. Donahue, C. George, A. H. Goldstein, J. F. Hamilton, H. Herrmann, T. Hoffmann, Y. Iinuma, M. Jang, M. E. Jenkin, J. L. Jimenez, A. Kiendler-Scharr, W. Maenhaut, G. McFiggans, T. F. Mentel, A. Monod, A. S. H. Prevot, J. H. Seinfeld, J. D. Surratt, R. Szmigielski and J. Wildt, The formation, properties and impact of secondary organic aerosol: current and emerging issues, *Atmos. Chem. Phys.*, 2009, **9**, 5155–5236.

21 P. J. Ziemann and R. Atkinson, Kinetics, products, and mechanisms of secondary organic aerosol formation, *Chem. Soc. Rev.*, 2012, **41**, 6582–6605.

22 V. F. McNeill, Aqueous organic chemistry in the atmosphere: sources and chemical processing of organic aerosols, *Environ. Sci. Technol.*, 2015, **49**, 1237–1244.

23 A. Virtanen, J. Joutsensaari, T. Koop, J. Kannosto, P. Yli-Pirila, J. Leskinen, J. M. Makela, J. K. Holopainen, U. Poeschl, M. Kulmala, D. R. Worsnop and A. Laaksonen, An amorphous solid state of biogenic secondary organic aerosol particles, *Nature*, 2010, **467**, 824–827.

24 Y. You, M. L. Smith, M. Song, S. T. Martin and A. K. Bertram, Liquid–liquid phase separation in atmospherically relevant particles consisting of organic species and inorganic salts, *Int. Rev. Phys. Chem.*, 2014, **33**, 43–77.

25 B. Wang, R. E. O'Brien, S. T. Kelly, J. E. Shilling, R. C. Moffet, M. K. Gilles and A. Laskin, Reactivity of liquid and semisolid secondary organic carbon with chloride and nitrate in atmospheric aerosols, *J. Phys. Chem. A*, 2015, **119**, 4498–4508.

26 M. L. Smith, Y. You, M. Kuwata, A. K. Bertram and S. T. Martin, Phase transitions and phase miscibility of mixed particles of ammonium sulfate, toluene-derived secondary organic material, and water, *J. Phys. Chem. A*, 2013, **117**, 8895–8906.

27 A. P. Ault, T. L. Guasco, O. S. Ryder, J. Baltrusaitis, L. A. Cuadra-Rodriguez, D. B. Collins, M. J. Ruppel, T. H. Bertram, K. A. Prather and V. H. Grassian, Inside *versus* outside: Ion redistribution in nitric acid reacted sea spray aerosol particles as determined by single particle analysis, *J. Am. Chem. Soc.*, 2013, **135**, 14528–14531.

28 D. J. Losey, R. G. Parker and M. A. Freedman, pH dependence of liquid–liquid phase separation in organic aerosol, *J. Phys. Chem. Lett.*, 2016, **7**, 3861–3865.

29 C. J. Ebben, A. P. Ault, M. J. Ruppel, O. S. Ryder, T. H. Bertram, V. H. Grassian, K. A. Prather and F. M. Geiger, Size-resolved sea spray aerosol particles studied by vibrational sum frequency generation, *J. Phys. Chem. A*, 2013, **117**, 6589–6601.

30 J. F. Davies and K. R. Wilson, Nanoscale interfacial gradients formed by the reactive uptake of OH radicals onto viscous aerosol surfaces, *Chem. Sci.*, 2015, **6**, 7020–7027.

31 S. Sobanska, J. Barbillat, M. Moreau, N. Nuns, I. De Waele, D. Petitprez, Y. Tobon and C. Bremard, Influence of stearic acid coating of the NaCl surface on the reactivity with NO_2 under humidity, *Phys. Chem. Chem. Phys.*, 2015, **17**, 10963–10977.

32 J. D. Raff, B. Njegic, W. L. Chang, M. S. Gordon, D. Dabdub, R. B. Gerber and B. J. Finlayson-Pitts, Chlorine activation indoors and outdoors *via* surface-mediated reactions of nitrogen oxides with hydrogen chloride, *Proc. Natl. Acad. Sci. U. S. A.*, 2009, **106**, 13647–13654.

33 G. Rubasinghege, S. Elzey, J. Baltrusaitis, P. M. Jayaweera and V. H. Grassian, Reactions on atmospheric dust particles: Surface photochemistry and size-dependent nanoscale redox chemistry, *J. Phys. Chem. Lett.*, 2010, **1**, 1729–1737.

34 G. Rubasinghege and V. H. Grassian, Role(s) of adsorbed water in the surface chemistry of environmental interfaces, *Chem. Commun.*, 2013, **49**, 3071–3094.

35 C. D. Hatch, K. M. Gierlus, J. D. Schuttlefield and V. H. Grassian, Water adsorption and cloud condensation nuclei activity of calcite and calcite coated with model humic and fulvic acids, *Atmos. Environ.*, 2008, **42**, 5672–5684.

36 L. Renbaum-Wolff, J. W. Grayson, A. P. Bateman, M. Kuwata, M. Sellier, B. J. Murray, J. E. Shilling, S. T. Martin and A. K. Bertram, Viscosity of α-pinene secondary organic material and implications for particle growth and reactivity, *Proc. Natl. Acad. Sci.*, 2013, **110**, 8014–8019.

37 J. P. Reid, A. K. Bertram, D. O. Topping, A. Laskin, S. T. Martin, M. D. Petters, F. D. Pope and G. Rovelli, The viscosity of atmospherically relevant organic particles, *Nat. Commun.*, 2018, **9**, 956.

38 J. F. Davies and K. R. Wilson, Raman spectroscopy of isotopic water diffusion in ultraviscous, glassy, and gel states in aerosol by use of optical tweezers, *Anal. Chem.*, 2016, **88**, 2361–2366.

39 D. J. Stewart, C. Cai, J. Nayler, T. C. Preston, J. P. Reid, U. K. Krieger, C. Marcolli and Y. H. Zhang, Liquid-liquid phase separation in mixed organic/inorganic single aqueous aerosol droplets, *J. Phys. Chem. A*, 2015, **119**, 4177–4190.

40 Y. Zhang, Y. Chen, A. T. Lambe, N. E. Olson, Z. Lei, R. L. Craig, Z. Zhang, A. Gold, T. B. Onasch, J. T. Jayne, D. R. Worsnop, C. J. Gaston, J. A. Thornton, W. Vizuete, A. P. Ault and J. D. Surratt, Effect of the aerosol-phase state on secondary organic aerosol formation from the reactive uptake of isoprene-derived epoxydiols (IEPOX), *Environ. Sci. Technol. Lett.*, 2018, **5**, 167–174.

41 A. L. Robinson, N. M. Donahue, M. K. Shrivastava, E. A. Weitkamp, A. M. Sage, A. P. Grieshop, T. E. Lane, J. R. Pierce and S. N. Pandis, Rethinking organic aerosols: Semivolatile emissions and photochemical aging, *Science*, 2007, **315**, 1259–1262.

42 N. M. Donahue, A. L. Robinson, C. O. Stanier and S. N. Pandis, Coupled partitioning, dilution, and chemical aging of semivolatile organics, *Environ. Sci. Technol.*, 2006, **40**, 2635–2643.

43 E. A. Stefaniak, A. Buczynska, V. Novakovic, R. Kuduk and R. Van Grieken, Determination of chemical composition of individual airborne particles by SEM/EDX and micro-Raman spectrometry: a review, *J. Phys.: Conf. Ser.*, 2009, **162**, 12019.

44 A. P. Ault, D. Zhao, C. J. Ebben, M. J. Tauber, F. M. Geiger, K. A. Prather and V. H. Grassian, Raman microspectroscopy and vibrational sum frequency generation spectroscopy as probes of the bulk and surface compositions of size-resolved sea spray aerosol particles, *Phys. Chem. Chem. Phys.*, 2013, **15**, 6206–6214.

45 J. M. Creamean, J. L. Axson, A. L. Bondy, R. L. Craig, N. W. May, H. Shen, M. H. Weber, K. A. Pratt and A. P. Ault, Changes in precipitating snow chemistry with location and elevation in the California Sierra Nevada, *J. Geophys. Res.: Atmos.*, 2016, **121**, 7296–7309.

46 R. L. Craig, A. L. Bondy and A. P. Ault, Computer-controlled Raman microspectroscopy (CC-Raman): a method for the rapid characterization of individual atmospheric aerosol particles, *Aerosol Sci. Technol.*, 2017, **51**, 1099–1112.

47 C. Deng, S. D. Brooks, G. Vidaurre and D. C. O. Thornton, Using Raman microspectroscopy to determine chemical composition and mixing state of airborne marine aerosols over the Pacific Ocean, *Aerosol Sci. Technol.*, 2014, **48**, 193–206.

48 S. Sobanska, G. Falgayrac, J. Rimetz-Planchon, E. Perdrix, C. Bremard and J. Barbillat, Resolving the internal structure of individual atmospheric aerosol particle by the combination of Atomic Force Microscopy, ESEM-EDX, Raman and ToF-SIMS imaging, *Microchem. J.*, 2014, **114**, 89–98.

49 A. L. Bondy, B. Wang, A. Laskin, R. L. Craig, M. V Nhliziyo, S. B. Bertman, K. A. Pratt, P. B. Shepson and A. P. Ault, Inland sea spray aerosol transport and incomplete chloride depletion: varying degrees of reactive processing observed during SOAS, *Environ. Sci. Technol.*, 2017, **51**, 9533–9542.

50 H. Rosen, A. D. A. Hansen, L. Gundel and T. Novakov, Identification of the optically absorbing component in urban aerosols, *Appl. Opt.*, 1978, **17**, 3859–3861.

51 H. Rosen and T. Novakov, Raman scattering and the characterisation of atmospheric aerosol particles, *Nature*, 1977, **266**, 708–710.

52 N. P. Ivleva, A. Messerer, X. Yang, R. Niessner and U. Pöschl, Raman microspectroscopic analysis of changes in the chemical structure and reactivity of soot in a diesel exhaust after treatment model system, *Environ. Sci. Technol.*, 2007, **41**, 3702–3707.

53 T. Catelani, G. Pratesi and M. Zoppi, Raman characterization of ambient airborne soot and associated mineral phases, *Aerosol Sci. Technol.*, 2014, **48**, 13–21.

54 O. Laskina, M. A. Young, P. D. Kleiber and V. H. Grassian, Infrared extinction spectroscopy and micro-Raman spectroscopy of select components of mineral dust mixed with organic compounds, *J. Geophys. Res.: Atmos.*, 2013, **118**, 6593–6606.

55 H.-J. Jung, H.-J. Eom, H.-W. Kang, M. Moreau, S. Sobanska and C.-U. Ro, Combined use of quantitative ED-EPMA, Raman microspectrometry, and ATR-FTIR imaging techniques for the analysis of individual particles, *Analyst*, 2014, **139**, 3949–3960.

56 S. Sobanska, H. Hwang, M. Choel, H. J. Jung, H. J. Eom, H. Kim, J. Barbillat and C. U. Ro, Investigation of the

chemical mixing state of individual Asian dust particles by the combined use of electron probe X-ray microanalysis and Raman microspectrometry, *Anal. Chem.*, 2012, **84**, 3145–3154.

57 J. De Gelder, K. De Gussem, P. Vandenabeele and L. Moens, Reference database of Raman spectra of biological molecules, *J. Raman Spectrosc.*, 2007, **38**, 1133–1147.

58 R. P. McLaughlin, B. Bird and P. J. Reid, Vibrational analysis of isopropyl nitrate and isobutyl nitrate, *Spectrochim. Acta, Part A*, 2002, **58**, 2571–2580.

59 A. L. Bondy, R. L. Craig, Z. Zhang, A. Gold, J. D. Surratt and A. P. Ault, Isoprene-derived organosulfates: Vibrational mode analysis by Raman spectroscopy, acidity-dependent spectral modes, and observation in individual atmospheric particles, *J. Phys. Chem. A*, 2018, **122**, 303–315.

60 E. Avzianova and S. D. Brooks, Raman spectroscopy of glyoxal oligomers in aqueous solutions, *Spectrochim. Acta, Part A*, 2013, **101**, 40–48.

61 M. C. Yeung and C. K. Chan, Water content and phase transitions in particles of inorganic and organic species and their mixtures using micro-Raman spectroscopy, *Aerosol Sci. Technol.*, 2010, **44**, 269–280.

62 Y. Chu, M. Sauerwein and C. K. Chan, Hygroscopic and phase transition properties of alkyl aminium sulfates at low relative humidities, *Phys. Chem. Chem. Phys.*, 2015, **17**, 19789–19796.

63 N. Jordanov and R. Zellner, Investigations of the hygroscopic properties of ammonium sulfate and mixed ammonium sulfate and glutaric acid micro droplets by means of optical levitation and Raman spectroscopy, *Phys. Chem. Chem. Phys.*, 2006, **8**, 2759–2764.

64 D. L. Bones, J. P. Reid, D. M. Lienhard and U. K. Krieger, Comparing the mechanism of water condensation and evaporation in glassy aerosol, *Proc. Natl. Acad. Sci.*, 2012, **109**, 11613–11618.

65 A. K. Y. Lee, T. Y. Ling and C. K. Chan, Understanding hygroscopic growth and phase transformation of aerosols using single particle Raman spectroscopy in an electrodynamic balance, *Faraday Discuss.*, 2008, **137**, 245–263.

66 A. K. Bertram, S. T. Martin, S. J. Hanna, M. L. Smith, A. Bodsworth, Q. Chen, M. Kuwata, A. Liu, Y. You and S. R. Zorn, Predicting the relative humidities of liquid-liquid phase separation, efflorescence, and deliquescence of mixed particles of ammonium sulfate, organic material, and water using the organic-to-sulfate mass ratio of the particle and the oxygen-to-carbon elemental ratio of the organic component, *Atmos. Chem. Phys.*, 2011, **11**, 10995–11006.

67 Q. Zhou, S.-F. Pang, Y. Wang, J.-B. Ma and Y.-H. Zhang, Confocal Raman studies of the evolution of the physical state of mixed phthalic acid/ammonium sulfate aerosol droplets and the effect of substrates, *J. Phys. Chem. B*, 2014, **118**, 6198–6205.

68 V. G. Ciobanu, C. Marcolli, U. K. Krieger, U. Weers and T. Peter, Liquid−liquid phase separation in mixed organic/inorganic aerosol particles, *J. Phys. Chem. A*, 2009, **113**, 10966–10978.

69 A. P. Ault, T. L. Guasco, J. Baltrusaitis, O. S. Ryder, J. V Trueblood, D. B. Collins, M. J. Ruppel, L. A. Cuadra-Rodriguez, K. A. Prather and V. H. Grassian, Heterogeneous reactivity of nitric acid with nascent sea spray aerosol: Large differences observed between and within individual particles, *J. Phys. Chem. Lett.*, 2014, **5**, 2493–2500.

70 A. K. Y. Lee and C. K. Chan, Single particle Raman spectroscopy for investigating atmospheric heterogeneous reactions of organic aerosols, *Atmos. Environ.*, 2007, **41**, 4611–4621.

71 K. J. Baustian, D. J. Cziczo, M. E. Wise, K. A. Pratt, G. Kulkarni, A. G. Hallar and M. A. Tolbert, Importance of aerosol composition, mixing state, and morphology for heterogeneous ice nucleation: a combined field and laboratory approach, *J. Geophys. Res.*, 2012, **117**, D06217.

72 J. D. Rindelaub, R. L. Craig, L. Nandy, A. L. Bondy, C. S. Dutcher, P. B. Shepson and A. P. Ault, Direct measurement of pH in individual particles *via* Raman microspectroscopy and variation in acidity with relative humidity, *J. Phys. Chem. A*, 2016, **120**, 911–917.

73 R. L. Craig, L. Nandy, J. L. Axson, C. S. Dutcher and A. P. Ault, Spectroscopic determination of aerosol pH from acid–base equilibria in inorganic, organic, and mixed systems, *J. Phys. Chem. A*, 2017, **121**, 5690–5699.

74 O. Laskina, H. S. Morris, J. R. Grandquist, Z. Qin, E. A. Stone, A. V Tivanski and V. H. Grassian, Size matters in the water uptake and hygroscopic growth of atmospherically relevant multicomponent aerosol particles, *J. Phys. Chem. A*, 2015, **119**, 4489–4497.

75 S. Schlucker, Surface-Enhanced Raman Spectroscopy: Concepts and Chemical Applications, *Angew. Chem., Int. Ed.*, 2014, **53**, 4756–4795.

76 K. Kneipp, Y. Wang, H. Kneipp, L. T. Perelman, I. Itzkan, R. Dasari and M. S. Feld, Single molecule detection using surface-enhanced Raman scattering (SERS), *Phys. Rev. Lett.*, 1997, **78**, 1667–1670.

77 E. L. Keller, N. C. Brandt, A. A. Cassabaum and R. R. Frontiera, Ultrafast surface-enhanced Raman spectroscopy, *Analyst*, 2015, **140**, 4922–4931.

78 S. L. Kleinman, R. R. Frontiera, A. I. Henry, J. A. Dieringer and R. P. Van Duyne, Creating, characterizing, and controlling chemistry with SERS hot spots, *Phys. Chem. Chem. Phys.*, 2013, **15**, 21–36.

79 S. Nie and S. R. Emory, Probing single molecules and single nanoparticles by surface-enhanced Raman scattering, *Science*, 1997, **275**, 1102–1106.

80 B. Sharma, R. R. Frontiera, A.-I. Henry, E. Ringe and R. P. Van Duyne, SERS: Materials, applications, and the future, *Mater. Today*, 2012, **15**, 16–25.

81 B. Sharma, M. F. Cardinal, S. L. Kleinman, N. G. Greeneltch, R. R. Frontiera, M. G. Blaber, G. C. Schatz and R. P. Van Duyne, High-performance SERS substrates: Advances and challenges, *MRS Bull.*, 2013, **38**, 615–624.

82 M. C. S. Pierre, P. M. Mackie, M. Roca and A. J. Haes, Correlating molecular surface coverage and solution-phase nanoparticle concentration to surface-enhanced

Raman scattering intensities, *J. Phys. Chem. C*, 2011, **115**, 18511–18517.

83 A. B. Zrimsek, N. Chiang, M. Mattei, S. Zaleski, M. O. McAnally, C. T. Chapman, A. I. Henry, G. C. Schatz and R. P. Van Duyne, Single-molecule chemistry with surface-and tip-enhanced Raman spectroscopy, *Chem. Rev.*, 2017, **117**, 7583–7613.

84 M. J. Ayora, L. Ballesteros, R. Perez, A. Ruperez and J. J. Laserna, Detection of atmospheric contaminants in aerosols by surface-enhanced Raman spectrometry, *Anal. Chim. Acta*, 1997, **355**, 15–21.

85 A. Sengupta, M. L. Laucks, N. Dildine, E. Drapala and E. J. Davis, Bioaerosol characterization of surface-enhanced Raman spectroscopy (SERS), *Aerosol Sci.*, 2005, **36**, 651–664.

86 K. Schwarzmeier, M. Knauer, N. P. Ivleva, R. Niessner and C. Haisch, Bioaerosol analysis based on a label-free microarray readout method using surface-enhanced Raman scattering, *Anal. Bioanal. Chem.*, 2013, **405**, 5387–5392.

87 R. L. Craig, A. L. Bondy and A. P. Ault, Surface enhanced Raman spectroscopy enables observations of previously undetectable secondary organic aerosol components at the individual particle level, *Anal. Chem.*, 2015, **87**, 7510–7514.

88 Y. Fu, C. Kuppe, V. K. Valev, H. Fu, L. Zhang and J. Chen, Surface-enhanced Raman spectroscopy: A facile and rapid method for the chemical component study of individual atmospheric aerosol, *Environ. Sci. Technol.*, 2017, **51**, 6260–6267.

89 J. Ofner, T. Deckert-Gaudig, K. A. Kamilli, A. Held, H. Lohninger, V. Deckert and B. Lendl, Tip-enhanced Raman spectroscopy of atmospherically relevant aerosol nanoparticles, *Anal. Chem.*, 2016, **88**, 9766–9772.

90 M. Gen and C. K. Chan, Electrospray surface-enhanced Raman spectroscopy (ES-SERS) for probing surface chemical compositions of atmospherically relevant particles, *Atmos. Chem. Phys.*, 2017, **17**, 14025–14037.

91 V. Sivaprakasam, M. B. Hart and J. D. Eversole, Surface enhanced Raman spectroscopy of individual suspended aerosol particles, *J. Phys. Chem. C*, 2017, **121**, 22326–22334.

92 N. Leopold and B. Lendl, A new method for fast preparation of highly surface-enhanced Raman scattering (SERS) active silver colloids at room temperature by reduction of silver nitrate with hydroxylamine hydrochloride, *J. Phys. Chem. B*, 2003, **107**, 5723–5727.

93 J. L. Axson, D. I. Stark, A. L. Bondy, S. S. Capracotta, A. D. Maynard, M. A. Philbert, I. L. Bergin and A. P. Ault, Rapid kinetics of size and pH-dependent dissolution and aggregation of silver nanoparticles in simulated gastric fluid, *J. Phys. Chem. C*, 2015, **119**, 20632–20641.

94 I. L. Bergin, L. A. Wilding, M. Morishita, K. Walacavage, A. P. Ault, J. L. Axson, D. I. Stark, S. A. Hashway, S. S. Capracotta, P. R. Leroueil, A. D. Maynard and M. A. Philbert, Effects of particle size and coating on toxicologic parameters, fecal elimination kinetics and tissue distribution of acutely ingested silver nanoparticles in a mouse model, *Nanotoxicology*, 2016, **10**, 352–360.

95 A. P. Ault, D. I. Stark, J. L. Axson, J. N. Keeney, A. D. Maynard, I. L. Bergin and M. A. Philbert, Protein corona-induced modification of silver nanoparticle aggregation in simulated gastric fluid, *Environ. Sci.: Nano*, 2016, **3**, 1510–1520.

96 P. A. Schueler, J. T. Ives, F. DeLaCroix, W. B. Lacy, P. A. Becker, J. Li, K. D. Caldwell, B. Drake and J. M. Harris, Physical structure, optical resonance, and surface-enhanced Raman scattering of silver-island films on suspended polymer latex particles, *Anal. Chem.*, 1993, **65**, 3177–3186.

97 E. C. Le Ru, E. Blackie, M. Meyer and P. G. Etchegoin, Surface enhanced Raman scattering enhancement factors: A comprehensive study, *J. Phys. Chem. C*, 2007, **111**, 13794–13803.

98 P. Larkin, *Infrared and Raman Spectroscopy; Principles and Spectral Interpretation*, Elsevier, Waltham, MA, 2011.

99 B. Jasse, R. S. Chao and J. L. Koenig, Laser Raman scattering in uniaxially oriented atactic polystyrene, *J. Polym. Sci., Polym. Phys. Ed.*, 1978, **16**, 2157–2169.

100 W. M. Sears, J. L. Hunt and J. R. Stevens, Raman scattering from polymerizing styrene. I. Vibrational mode analysis, *J. Chem. Phys.*, 1981, **75**, 1589–1598.

101 A. Laskin, M. K. Gilles, D. A. Knopf, B. Wang and S. China, Progress in the analysis of complex atmospheric particles, *Annu. Rev. Anal. Chem.*, 2016, **9**, 117–143.

102 P. Venkateswarlu, H. D. Bist and Y. S. Jain, Laser excited Raman spectrum of ammonium sulfate single crystal, *J. Raman Spectrosc.*, 1975, **3**, 143–151.

103 P. V. Jentzsch, B. Kampe, V. Ciobota, P. Roesch and J. Popp, Inorganic salts in atmospheric particulate matter: Raman spectroscopy as an analytical tool, *Spectrochim. Acta, Part A*, 2013, **115**, 697–708.

104 D. L. Rousseau, R. E. Miller and G. E. Leroi, Raman spectrum of crystalline sodium nitrate, *J. Chem. Phys.*, 1968, **48**, 3409–3413.

105 S. Gajaraj, C. Fan, M. Lin and Z. Hu, Quantitative detection of nitrate in water and wastewater by surface-enhanced Raman spectroscopy, *Environ. Monit. Assess.*, 2013, **185**, 5673–5681.

106 K. H. Michaelian, The Raman spectrum of kaolinite #9 at 21 °C, *Can. J. Chem.*, 1986, **64**, 285–289.

107 R. L. Frost, Fourier transform Raman spectroscopy of kaolinite, dickite, and halloysite, *Clays Clay Miner.*, 1995, **43**, 191–195.

108 R. L. Frost, T. Thu Ha and J. Kristof, FT-Raman spectroscopy of the lattice region of kaolinite and its intercalates, *Vib. Spectrosc.*, 1997, **13**, 175–186.

109 J. de Villepin and A. Novak, Vibrational spectra of and isotope effect in hydrogen bonded potassium hydrogen oxalate, *Spectrosc. Lett.*, 1971, **4**, 1–8.

110 J. L. Koenig and A. C. Angood, Raman spectra of poly(ethylene glycols) in solution, *J. Polym. Sci., Part A-2*, 1970, **8**, 1787–1796.

